How to cite: *Angew. Chem. Int. Ed.* **2022,** *61,* e202206613
International Edition: doi.org/10.1002/anie.202206613
German Edition: doi.org/10.1002/ange.202206613

Metal–Organic Frameworks

CO_2 Capture by Hybrid Ultramicroporous TIFSIX-3-Ni under Humid Conditions Using Non-Equilibrium Cycling

Saif Ullah[+], Kui Tan[+], Debobroto Sensharma[+], Naveen Kumar, Soumya Mukherjee, Andrey A. Bezrukov, Jing Li, Michael J. Zaworotko,* and Timo Thonhauser**

Abstract: Although pyrazine-linked hybrid ultramicroporous materials (HUMs, pore size <7 Å) are benchmark physisorbents for trace carbon dioxide (CO_2) capture under dry conditions, their affinity for water (H_2O) mitigates their carbon capture performance in humid conditions. Herein, we report on the co-adsorption of H_2O and CO_2 by TIFSIX-3-Ni—a high CO_2 affinity HUM—and find that slow H_2O sorption kinetics can enable CO_2 uptake and release using shortened adsorption cycles with retention of ca. 90 % of dry CO_2 uptake. Insight into co-adsorption is provided by in situ infrared spectroscopy and ab initio calculations. The binding sites and sorption mechanisms reveal that both CO_2 and H_2O molecules occupy the same ultramicropore through favorable interactions between CO_2 and H_2O at low water loading. An energetically favored water network displaces CO_2 molecules at higher loading. Our results offer bottom-up design principles and insight into co-adsorption of CO_2 and H_2O that is likely to be relevant across the full spectrum of carbon capture sorbents to better understand and address the challenge posed by humidity to gas capture.

Introduction

The continued production of greenhouse gases, coupled with the energy demands of the chemical industry ($\approx$15 % of global energy consumption, with a projected threefold increase in demand for chemical commodities by 2050), require effective carbon capture and remediation technologies.[1] Liquid amines[2] and amine-grafted porous materials[3] remain the state-of-the-art for carbon capture despite relying upon chemisorption to capture CO_2, thereby suffering from a high energy footprint and slow kinetics, especially for trace CO_2 remediation.[4,5] CO_2 selective physisorbents that overcome this issue by significantly lowering the energy needed to recycle the sorbent include metal–organic materials (MOMs) and zeolites. The presence of unsaturated metal centers and/or functionalization by organic amines means that MOMs, including metal-organic frameworks (MOFs), can exhibit high CO_2 selectivity.[4,6,7] Carbon capture performance is often mitigated by the presence of other components in gas feeds.[8] In this context, the ubiquity of water vapor in downstream feedstocks arguably makes it the biggest concern, not only because of the generally poor water stability of many MOFs,[9] but also because water adsorption can overwhelm CO_2 affinity in porous physisorbents.[10] This is largely because H_2O, with its smaller dimensions and permanent dipole, can be more readily adsorbed into most pores, outcompeting CO_2 and other gaseous adsorbates for the strongest binding site(s). In addition, hydrolytic instability means that the separation performance of industrially relevant gas mixtures often deteriorates over successive cycles.[10] Two challenges, therefore, handicap the development of CO_2-selective physisorbents: i) the dearth of adsorbents that combine strong carbon capture performance with low water uptake; ii) lack of knowledge about mechanisms of CO_2 and H_2O co-adsorption. These challenges are intertwined in that knowledge gained in one will likely inform and guide the other. A number of strategies have been exploited to address these challenges with varying degrees of success,[6,11,12] such as tethering heteroatom-containing species on unsaturated metal centers,[13] introducing active sites onto metal building units as termini or capping ligands,[14,15] or incorporation of alkylamine functionalities into linker components of existing MOFs.[16]

[*] Dr. S. Ullah,[+] Prof. T. Thonhauser
Department of Physics and Center for Functional Materials,
Wake Forest University
Winston-Salem, NC 27109 (USA)
E-mail: ullahs@wfu.edu
thonhauser@wfu.edu
Dr. K. Tan[+]
Department of Materials Science & Engineering,
University of Texas at Dallas
Richardson, TX 75080 (USA)
Dr. D. Sensharma,[+] Dr. N. Kumar, Dr. S. Mukherjee,
Dr. A. A. Bezrukov, Prof. M. J. Zaworotko
Bernal Institute, Department of Chemical Sciences,
University of Limerick
Limerick V94 T9PX (Ireland)
E-mail: xtal@ul.ie
Prof. J. Li
Department of Chemistry and Chemical Biology,
Rutgers University
Piscataway, NJ 08854 (USA)
[+] These authors contributed equally to this work.

Hybrid ultramicroporous materials (HUMs) are of particular interest in the context of trace carbon capture because of their ultra-high selectivity for CO_2 over N_2[17,18] and CH_4 but their performance is typically reduced by co-adsorption of H_2O.[18,19] The prototypal HUM with respect to trace carbon capture, SIFSIX-3-Zn, $[Zn(pyz)_2(SiF_6)]_n$ (3 = pyrazine = pyz), is sustained by pillaring Zn^{II}-pyz square grids using SiF_6^{2-} (SIFSIX) anions.[17] An ultramicropore of 3.84 Å diameter and strong electrostatic interactions between SiF_6^{2-} and CO_2 resulted in SIFSIX-3-Zn setting a benchmark for S_{CN} (CO_2/N_2 adsorption selectivity) of $\approx$1800, almost an order of magnitude higher than earlier benchmarks and two orders of magnitude above most MOFs.[17] Isostructural variants (SIFSIX-3-Cu, Ni, and Co)[18,20,21] can further improve carbon capture performance in the low-pressure region (<10000 ppm).[22] The CO_2 uptake of SIFSIX-3-Ni in the presence of moisture[23,24] under simulated flue-gas conditions (0.15 bar CO_2, 0.85 bar N_2, 75 % RH) was found to be 62 % of that under dry conditions.[18,25]

Hydrolytic stability of SIFSIX HUMs was enhanced by replacing the SIFSIX pillars with TiF_6^{2-}. TIFSIX-3-Ni was found to retain stability at 80 % RH whereas SIFSIX-3-Ni[25] underwent a moisture-induced phase transformation at ca. 50 % RH.[26] In addition to enhanced stability, TIFSIX-3-Ni exhibited higher CO_2 uptake vs. SIFSIX-3-Ni under the same conditions, resulting in enhanced CO_2/N_2 selectivity and 83 % of the dry CO_2 uptake.[18,25] Recent studies concluded that TIFSIX-3-Ni outperforms SIFSIX-3-Ni and NbOFFIVE-1-Ni for trace carbon capture under real-world conditions.[24,25]

Despite the high number of MOF platforms studied for carbon capture, e.g., the UiO-66 and MOF-74 families to name a couple,[27–30] MOFs have typically been examined for post-combustion capture since they tend to suffer from negligible CO_2 uptakes at the low partial pressures relevant to direct air capture (DAC).[18] Among MOFs, CALF-20 stands out as a selective ($S_{CN} \approx 230$ for $CO_2:N_2 = 10:90$), stable, inexpensive, and scalable sorbent that sets the standard for postcombustion CO_2 capture.[31] With respect to physisorbents that appreciably adsorb CO_2 at partial pressures below 430 ppm TIFSIX-3-Ni remains a benchmark material with a CO_2 uptake of 1.2 mmol g^{-1} at 500 ppm, and an ultrahigh S_{CN} of 8090 at 500 ppm/1 bar.

The effect of humidity upon sorbent performance is a crucial performance parameter as exemplified by TIFSIX-3-Ni and CALF-20, for which H_2O tends to have a parasitic effect upon CO_2 uptake above a threshold relative humidity. However, instances of cooperative effects between CO_2 and H_2O are known in amine-functionalized MOFs.[13] A recent review summarized CO_2 adsorption in the presence of moisture by various materials including MOFs, zeolites, and amine-functionalized porous solids.[10] Nevertheless, whereas HUMs have the potential to address carbon capture in the presence of humidity as observed in dynamic column breakthrough measurements (DCB),[24] the mechanisms of CO_2 and H_2O co-adsorption remain unaddressed. Such insight is inaccessible via gravimetric/volumetric isotherms or equilibrium DCB measurements alone but can be gained through in situ studies and computational modeling. In this paper, we combine DCB and TPD experiments in the presence of moisture with in situ infrared spectroscopy and ab initio calculations to address the kinetics and thermodynamics of CO_2 and H_2O co-adsorption in TIFSIX-3-Ni.

Results and Discussion

In order to experimentally determine the effect of moisture on the adsorption of CO_2 by TIFSIX-3-Ni, a series of mixed-gas adsorption and desorption experiments were conducted using dry and moist gas streams. The pure component gas uptake of CO_2 was found by a dry single-component DCB experiment to be 55 $cm^3 g^{-1}$, which equates to 0.95 molecules per unit cell (Figure S1). This value is in excellent agreement with the theoretical saturation of 1 molecule per unit cell. Similarly, using a nitrogen stream saturated with humidity (ca. 95 % R.H., 3 % v/v) we determined an equilibrium H_2O uptake of ca. 240 $cm^3 g^{-1}$, which equates to 4.1 molecules per unit cell (Figure 1a). This value agrees with the previously reported saturation amount of 4 molecules per unit cell. N_2 adsorption was assumed to be negligible.

Subsequently, we conducted a DCB experiment using a moisture-saturated stream of CO_2 (75 % R.H., 2.25 % v/v). Due to the low molar ratio of water present, we observed a large discrepancy in breakthrough times for H_2O and CO_2 (ca. 5 min g^{-1} for CO_2, ca. 300 min g^{-1} for H_2O) (Figure 1b). Although the breakthrough time for CO_2 in wet and dry experiments was found to be similar, the significant "roll-up" above $C/C_0 = 1$ of the CO_2 signal with the cumulative adsorption of water indicates that the initially adsorbed CO_2 is gradually displaced as the water-saturated front slowly advances through the solid fixed bed with increasing time and water loading. A similar effect has been described in Zeolite 13X and was attributed to a discrepancy between the kinetics of adsorption of CO_2 and H_2O on the fixed bed, rather than an overall equilibrium co-operative or thermodynamic effect, wherein water permeates the bed slowly and CO_2 permeates rapidly.[32,33] The detrimental effect of humidity on adsorption is dependent on the quantity of water to which the fixed bed is exposed, and—due to this difference in kinetics—therefore depends on the duration of the adsorption branch of the experiment. CO_2 adsorbed by the portion of TIFSIX-3-Ni into which the H_2O front has not permeated is effectively adsorbed into a "dry" adsorbent, only to be displaced as the front moves further along the direction of flow.

This interpretation is supported by temperature-programmed desorption (TPD) experiments (Figure 1c,d). TPD after saturation of TIFSIX-3-Ni with pure CO_2 shows that heating the adsorbent bed to 120 °C under a helium flow of 20 sccm enables recovery of 55.0 $cm^3 g^{-1}$ of CO_2 within 100 min g^{-1}. However, TPD conducted under similar conditions after full saturation with humid CO_2 over several hours (determined by water breaking through the column) recovered only 15.7 $cm^3 g^{-1}$ of CO_2 (0.27 molecules per unit cell), and ca. 240 $cm^3 g^{-1}$ of H_2O. As such, we postulate that following the completion of H_2O breakthrough with zero

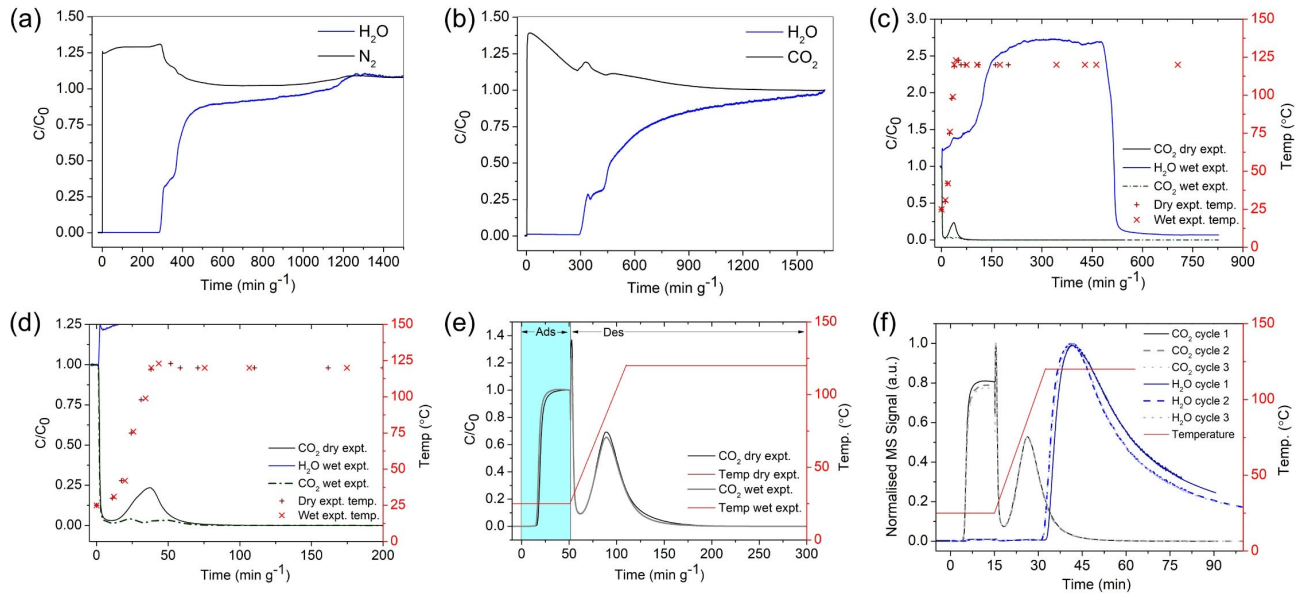

Figure 1. Wet gas DCB curves for a) N_2 (20 sccm), b) CO_2 (10 sccm) saturated with moisture. c) TPD under 20 sccm of He of CO_2 adsorbed under dry and wet conditions, d) zoomed in to show CO_2 profiles. e) A comparison of adsorption and desorption curves for breakthrough of dry and wet CO_2 with shortened adsorption branches. f) A comparison of three cycles of adsorption and desorption curves for breakthrough of wet CO_2 with shortened adsorption branches.

slope, which would require an infeasible experimental duration, no CO_2 is retained in the TIFSIX-3-Ni bed. Comparing the TPD data with and without the presence of moisture shows that under equilibrium conditions CO_2 and H_2O compete for binding sites in TIFSIX-3-Ni. However, these experiments also show that the different rates of saturation of CO_2 and H_2O play a crucial role in determining the quantity of CO_2 and H_2O present across the adsorbent bed at any time prior to full saturation by moisture.

In order to explore the implications of this finding for the use of TIFSIX-3-Ni in capturing CO_2 from moist gas streams, we conducted a pair of dry and wet experiments consisting of successive adsorption-desorption cycles with short adsorption times to study CO_2 adsorption before saturation of the TIFSIX-3-Ni bed by H_2O (Figure 1e, Figure S2). Desorption was conducted over several hours by heating to 120 °C under a He flow of 20 sccm. In these experiments, we found that breakthrough adsorption and desorption traces using dry and wet CO_2 resulted in similar profiles and minimal reduction in uptakes arising from the presence of moisture. For example, at a flow rate of 3 sccm breakthrough times of ca. 18 and 16 min g^{-1} were determined from the adsorption branches of the first cycle of dry and wet experiments, respectively. These values correspond to CO_2 uptakes of 53.9 $cm^3 g^{-1}$ and 48.2 $cm^3 g^{-1}$. Importantly, desorbed CO_2 amounts were determined to be 54 and 46 $cm^3 g^{-1}$ from the TPD branches succeeding the respective adsorption branches, showing that displacement of CO_2 by water played a minimal role under these conditions. Subsequent second and third cycles conducted after adsorption of humid CO_2 and combined TPD + regeneration steps at 120 °C showed similar adsorption and desorption profiles for CO_2, implying that any induced phase transformations are fully reversed during regeneration (Figure 1f, Figure S3). Uptakes for the second and third cycles from the adsorption branch were found to be 50.8 and 51.2 $cm^3 g^{-1}$, and therefore appeared to stabilise after the first cycle. Notably, H_2O adsorbed during the wet adsorption cycles was qualitatively detectable in mass spectrometry signals during these cycles, and similar to CO_2 adsorption, showed a stable profile by the second cycle. This modest effect of humidity on CO_2 uptake, especially the low displacement of CO_2 by water during shortened adsorption cycle, suggests that co-adsorption of CO_2 and H_2O has a different mechanism than MOFs such as MOF-74 and HKUST-1.[27,34]

In light of these findings, the strong CO_2 sorption under non-equilibrium and low-H_2O loading states suggest that a short-cycling based solution could enable improved performance for capture and release of CO_2 from wet gas streams. Understanding the interactions between CO_2, H_2O, and the TIFSIX-3-Ni framework would provide insight into adsorption of CO_2 by TIFSIX-3-Ni under wet conditions. To uncover the mechanisms involved, we conducted in situ FTIR experiments on TIFSIX-3-Ni upon exposure to humid CO_2 (pure CO_2 adsorption in TIFSIX-3-Ni was reported previously).[35] The gas-phase signal is prohibitively high above pressures of 20 Torr (saturation of the detector) making it difficult to distinguish adsorbed CO_2 from gas-phase CO_2. For the single-phase CO_2 study, an activated TIFSIX-3-Ni sample was first exposed to ≈760 Torr of CO_2 for adsorption saturation and then evacuated by pumping the cell. Within ≈5 seconds of evacuation, the pressure of gas-phase CO_2 dropped below ≈500 mTorr (negligible gas-phase IR absorption). The spectra were recorded as a function of time during the desorption process (see Figure S4). The characteristic asymmetric stretching ν_{as} band of

adsorbed CO_2 within TIFSIX-3-Ni was detected at 2342 cm^{-1} upon evacuating the headspace. In addition, a ν_{as} band of trace amounts of naturally occurring $C^{13}O_2$ is also noticeable at 2273 cm^{-1}. Although adsorbed CO_2 is rapidly desorbed upon heating in TPD experiments, under these conditions the adsorbed CO_2 exhibits a slow desorption rate upon evacuation under vacuum, i.e., the intensity of the $\nu_{as}(CO_2)$ band decreases only by ≈35 % within ≈100 min at room temperature,[35] allowing us to investigate the effect of H_2O exposure on the concentration of trapped CO_2.

For the CO_2 and H_2O co-adsorption study, we first loaded pure CO_2 inside TIFSIX-3-Ni at a pressure of ≈760 Torr. After the adsorption reached saturation, the headspace was evacuated for ≈1 h. ≈75 % of CO_2 was still trapped inside the material as determined by measuring the intensity of the $\nu_{as}(CO_2)$ band at 2342 cm^{-1} and the combination $\nu_{as}+\nu_s$ band at 3699 cm^{-1} (bottom (lime) spectrum in the middle panel of Figure 2). A notable perturbation of characteristic pyz linker bands including ν(CH), $\nu(CC)_{phenyl}$, $\nu(CN)_{phenyl}$, δ_{ip}(CH) and δ(ring) was observed in the difference spectrum, providing evidence that CO_2 interacts with the pyz linker in addition to the primary F binding sites. Water vapor alone was then introduced into the vacuum cell as a function of pressure up to ≈14 Torr. Adsorption of water was characterized by the growth of its stretching and bending bands $\nu(H_2O)$ and $\beta(H_2O)$, centered at 3530 and 1660 cm^{-1} (middle panel Figure 2). Interestingly, the $\nu_{as}(CO_2)$ band does not decrease upon loading H_2O as evident in the evolution of its integrated area shown in Figure S5 and differential spectra in Figure 2. Even prolonged water exposure for up to ≈1 h at 14 Torr did not result in a significant loss of CO_2, outlining the difference in the affinity for co-adsorption under low- and high-loading regimes. The retention of CO_2 in TIFSIX-3-Ni differs from previous observations in other MOFs such as MOF-74 and HKUST-1, which readily lose adsorbed CO_2 upon exposure to ≈8 Torr water vapor at room temperature;[27,34] the loss of CO_2 in these MOFs has been attributed to a molecular exchange between CO_2 and H_2O at the unsaturated metal centers.[27] Differential spectra in Figure 2 reveal that water inclusion induces significantly higher perturbations to the pyz linker bands including ν(CH), coupled ν(CC)/$\delta(CH)_{ip}$ and $\delta(CH)_{ip}$/ν(CC)/δ(ring) vibrations. This suggests interaction between H_2O and the organic linker, as verified by computational studies below.

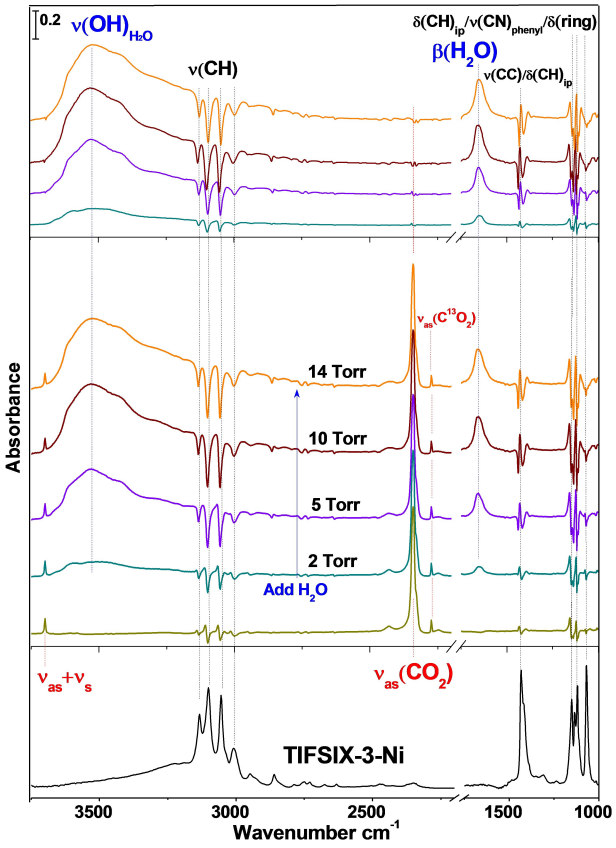

Figure 2. IR spectra showing the loading of H_2O into TIFSIX-3-Ni with pre-loaded CO_2. Bottom panel: Spectrum of activated TIFSIX-3-Ni under vacuum (<20 mTorr), referenced to the KBr pellet. Middle panel: Difference spectra showing the loading of CO_2 (bottom lime line) and subsequent H_2O vapor (top four lines) into TIFSIX-3-Ni; each is referenced to the activated sample under vacuum. The pressures were retained for ≈3 min each at ≈2, 5 and 10 Torr; for ≈1 h at ≈14 Torr. Top panel: Differential spectra showing the increase of H_2O bands and evolution of CO_2 bands by referencing spectra after loading H_2O to the spectrum of TIFSIX-3-Ni containing only pre-loaded CO_2 (see the lime line in the middle panel). Notations and acronyms: ν = stretching, β = scissoring, δ = deformation, ip = in plane.

While it has been reported that CO_2 and H_2O are co-adsorbed in TIFSIX-3-Ni and related materials through isotherm measurements,[25] these results cannot conclusively determine whether the molecules occupy the same pore or segregate into different pores. Crystallographic evidence would be the most direct proof for the co-inhabitation of CO_2 and H_2O in the same pore; however, it is extremely difficult to obtain single crystals of TIFSIX-3-Ni by current preparation methods such as solvent diffusion and solvothermal synthesis. To provide a definitive answer to this question, we further analyzed our in situ IR results. Upon loading water, the $\nu_{as}(CO_2)$ band does not exhibit an appreciable decrease in intensity but slight perturbation characterized by the derivative feature in the differential IR spectra (Figure S6), which points to the interactions of pre-adsorbed CO_2 with the incoming H_2O molecules. This evidence, for the first time, indicates that H_2O and CO_2 are located in the same pore when co-adsorbing. The ultramicropore size of 3.25 Å in TIFSIX-3-Ni (see Supporting Information and Figure S12 for further details) is significantly smaller compared to most other porous systems.[36–38] With in situ IR evidence of simultaneous binding in the same pore, the mechanisms that allow for such an effective accommodation of multiple molecules (one CO_2 plus adsorbed H_2O) in such a small pore has deep implications for multi-component adsorption in other ultramicroporous materials and may prove an important consideration in the future design of CO_2-capture adsorbents.

In order to articulate a mechanism correlating these intriguing effects, we further investigated the molecular adsorption/co-adsorption via ab initio calculations. For full loading by single-component adsorption, we found total

binding energies of 0.83 eV for one CO_2 per unit cell and 2.55 eV for four H_2O per unit cell, in good agreement with the full-cycle breakthrough data presented (Table 1).[25] Intriguingly however, we find that for the adsorption of a single water molecule in a unit cell of TIFSIX-3-Ni, the binding energy is 0.67 eV, lower than that for CO_2. This suggests that at lower water loadings, affinity for CO_2 may match or even exceed that towards water in TIFSIX-3-Ni. Energies determined for the binding of CO_2 and H_2O into the same ultramicropore show a surprising favorability towards co-adsorption, with values of 1.289, 1.703, and 2.255 eV corresponding to co-adsorbed states containing one CO_2 molecule and one, two, and three H_2O molecules, respectively. Remarkably, the value of 2.255 eV for CO_2+3H_2O co-adsorbed is lower by a small margin than the value of 2.55 eV for the saturation of pure water uptake of $4\,H_2O$, showing that although the eventual saturation of the void space with water is thermodynamically favored, the energy of co-adsorbed configurations closely approaches those of this state. Furthermore, a similar interaction is found in another isostructural SIFSIX-3-Ni. The binding energy for H_2O and CO_2 in SIFSIX-3-Ni is 0.623 and 0.79 eV, respectively, slightly weaker than in TIFSIX-3-Ni. The larger host-guest separations explain the weaker binding energies of H_2O and CO_2 in SIFSIX-3-Ni in comparison with TIFSIX-3-Ni (see Figure S24).

A key observation here is that this co-adsorption is "non-competitive" in the sense that the molecules do not compete for the same site, but rather CO_2 occupies the center of the pore whereas H_2O binds along the edge, providing enough room and effectively avoiding a crossing of their "private space" (Figure 3). We further analyze the binding interactions through induced charge densities, i.e., charge density rearrangements upon loading of the guest molecules (see Figure 4). H_2O is found to interact with two F atoms via H···F bonding with a 1.922 Å H···F distance. In addition, a strong interaction with the pyz linkers is also evident, in agreement with the strong perturbation of the pyz ring modes including ν(CH), coupled ν(CC)/$\delta(CH)_{ip}$ and $\delta(CH)_{ip}/\nu(CC)/\delta$(ring) vibrations (upon water exposure) observed in our in situ differential IR spectra in Figures 2. For CO_2, we see a stronger interaction between C_{CO2} and the four equatorial F atoms with C···F distances of 3.10 Å,

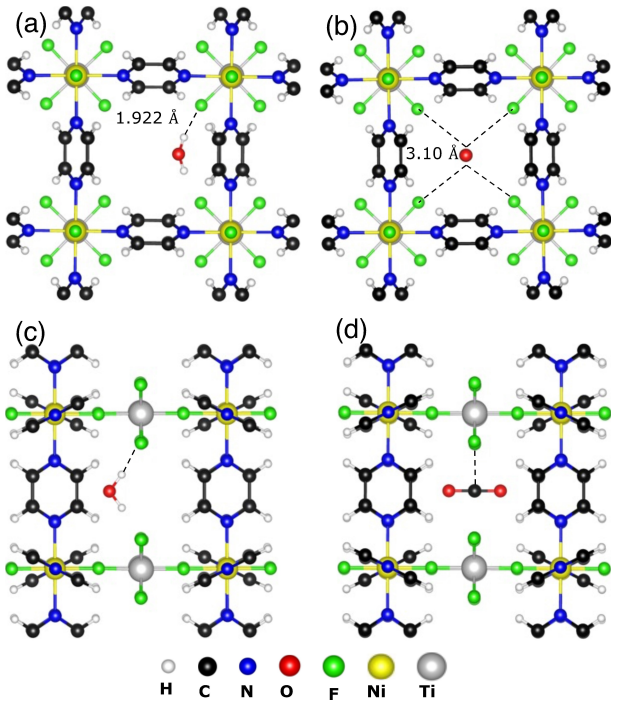

Figure 3. Top (along the pore channel) and side (across the pore channel) views of the binding locations for single-component adsorption of H_2O (a, c) and CO_2 (b, d) in TIFSIX-3-Ni. One guest molecule per unit cell was adsorbed. The solid spheres at the bottom label the various atomic species in TIFSIX-3-Ni.

accounting for the strong binding affinity of CO_2.[35] In addition, weaker interactions of CO_2 with the pyz linker were also observed; these interactions account for the perturbations of phenyl ring modes observed in our in situ IR spectra in Figure 2 and are also confirmed by the slight changes induced in pyz···pyz separation upon CO_2 loading (see Figure S18).

The different binding sites for H_2O and CO_2 are key to explaining their co-adsorption in the same pore (see Figure 5). In co-adsorption, we investigate both possibilities, e.g., introducing H_2O to a pre-adsorbed CO_2 and vice versa, and find that the optimum binding positions are independent of the loading preference. Both guest molecules remain

Table 1: Total binding energy [eV], incremental binding energy [eV], and binding energy per molecule [eV] for various guest molecules in TIFSIX-3-Ni. We studied the effects of adding up to 3 water molecules since this is the experimentally observed upper loading limit per unit cell in the presence of CO_2 observed in our in situ IR measurements. NB refers to "no binding".

Guest molecules	Total binding energy	Incremental binding energy	Binding energy per molecule
CO_2	0.830	0.830	0.830
$2\,CO_2$	NB	NB	NB
$CO_2+1\,H_2O$	1.289	0.459	0.644
$CO_2+2\,H_2O$	1.703	0.414	0.567
$CO_2+3\,H_2O$	2.255	0.552	0.564
$1\,H_2O$	0.670	0.670	0.670
$2\,H_2O$	1.209	0.539	0.604
$3\,H_2O$	1.802	0.593	0.601
$4\,H_2O$	2.555	0.753	0.639
$5\,H_2O$	NB	NB	NB

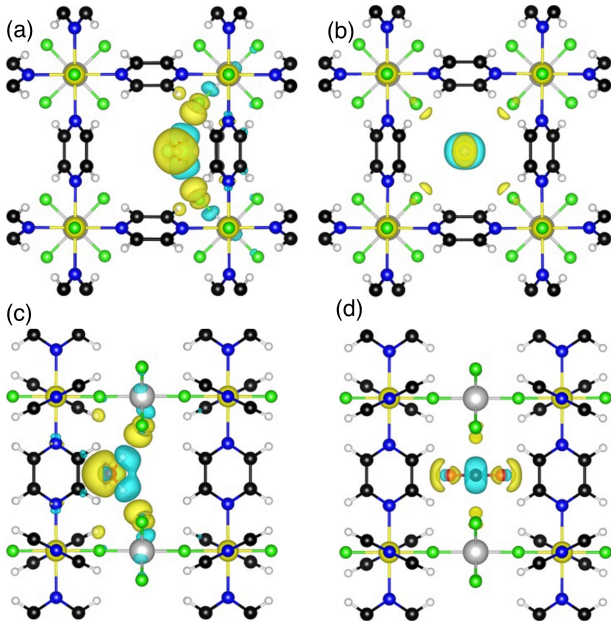

Figure 4. Induced charge densities for single-component adsorption of H_2O (a, c) and CO_2 (b, d) in TIFSIX-3-Ni at an iso-level of 1×10^{-3} eÅ^{-3}. One guest molecule per unit cell was adsorbed. Clear interactions between the guest molecules and the F atoms are visible. Color coding as in Figure 3.

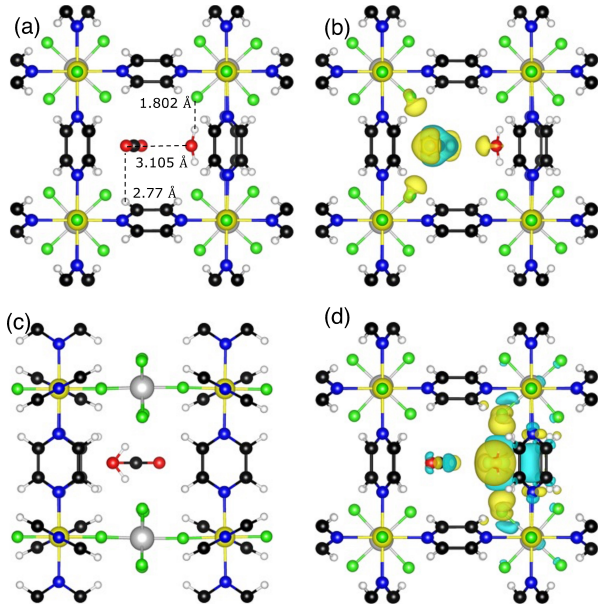

Figure 5. The left panel (a, c) shows the front and side views of one H_2O and one CO_2 molecule co-adsorbed in the TIFSIX-3-Ni unit cell. The right panel (b, d) shows induced charge density plots for co-adsorption of CO_2 and H_2O. The induced density of CO_2 is plotted against preloaded H_2O (b) and the density induced by H_2O against preloaded CO_2 (d). The co-adsorbed species are involved in a "duet" which is clearly visible from the uncommon interaction resulting in rare-occurring synergistic effects. Color coding of atoms as in Figure 3 and iso-values as in Figure 4.

almost at their optimum single-component binding positions without a deterioration in CO_2 binding energy as rapid as that observed in MOF-74 and HKUST-1 (at ≈8 Torr and room temperature).[27,34] In TIFSIX-3-Ni, due to the absence of open-metal sites and different preferential binding positions, CO_2 is less affected by the presence of H_2O. This observation is consistent with that in SIFSIX-3-Ni (see Figures S8 and S9). Due to the small pore size, we do see a slight bending/rotation of the CO_2 and a marginal displacement of H_2O towards the pyz ring (also seen by the additional charge transfer between H_2O and the pyz rings of TIFSIX-3-Ni in Figure 5) to allow both molecules to best fit in at their respective binding sites. The intermolecular distance (measured between O···O) is calculated to be 3.105 Å. This results in the shortening of the H_{H_2O}···F distances to 1.802 Å. In the same manner, due to the slight bending of CO_2, the C_{CO_2}···F contacts are elongated on one side to 3.833 Å and shortened on the opposite side to 2.73 Å. One O_{CO_2} atom is 2.77 Å from the H atoms of the pyz rings on top and bottom, providing extra support for the stable binding of CO_2 even in the presence of H_2O.

Table 1 gives the energetics of co-adsorption. The total binding energy for co-adsorption is 1.289 eV, which is favorable compared to the individual binding energies of 0.83 eV for CO_2 and 0.67 for H_2O. Of particular interest is the incremental binding energy of 0.459 eV when adsorbing H_2O next to a pre-adsorbed CO_2, a remarkable energy gain of co-adsorption in the same pore that is contrary to the typical competitive behavior between sorbates. Surprisingly, the O···C separation of H_2O and CO_2 in the same pore is just 2.95 Å, giving rise to a rare and unexpected synergistic interaction[39,40] as indirectly evidenced by the slight perturbation of the $\nu(CO_2)$ band shown in the differential spectra of Figure 2 (also see Figure S6). We can quantify this effect by calculating the hypothetical single-component adsorption energy for both guest molecules, but in their (metastable) co-adsorption structural configurations. This results in a hypothetical binding energy of 0.599 eV for CO_2 and 0.601 eV for H_2O (a noticeable decrease from the true binding energies in Table 1). The synergistic attractive interaction between the two guest molecules is thus $1.289-(0.599+0.601)=0.089$ eV. The effect of adding a H_2O to a pre-adsorbed CO_2 can also be seen in Figure 5, where we show the induced charge density of this process (we also show the case of adding a CO_2 to a pre-adsorbed water); the synergistic interaction between CO_2 and H_2O becomes clearly visible. Table 1 shows that co-adsorption is favorable at low water loading as the total binding energy of CO_2+1 H_2O (1.289 eV) is more favorable than the binding energy of $2H_2O$ (1.209 eV). However, at higher water loading, the formation of a water framework is observed and the binding energy for $3H_2O$ (1.802 eV) becomes slightly more favorable than CO_2+2H_2O (1.703 eV), which is in agreement with our observations from DCB and TPD experiments, in which the effective water loading increases with the quantity of wet CO_2 that flows over the TIFSIX-3-Ni bed.

Finally, we studied the inclusion of more than one water molecule with the CO_2 concentration kept fixed since

TIFSIX-3-Ni can only adsorb one CO_2 per pore. Due to the larger kinetic diameter of CO_2 the energy of more than one molecule per pore becomes unfavorable, making it impossible to accommodate two CO_2 per pore (see Figures S26 and S27 and Table 1). The fact that 3 H_2O (in case of co-adsorption) and 4 H_2O can be accommodated per pore is due to the formation of a water cluster discussed below. However, when a 5th H_2O is added to a pore, the binding energy also becomes repulsive (Figure S27, Table 1). The model of 3 H_2O and 1 CO_2 within one unit cell corresponds to the experimental condition of loading at 14 Torr H_2O into TIFSIX-3-Ni with pre-adsorbed CO_2 as shown in Figures 2, S7, and S10. Binding configurations are shown in Figures S19 and S20. Table 1 shows that adding two or three water molecules to a pre-adsorbed CO_2 is energetically still favorable, which is surprising for the small size of this ultramicropore. For the case of two water molecules, this is made possible through a noticeable spatial separation/arrangement (Figure S19) with a significant incremental binding energy of 0.414 eV. However, for the case of three added water molecules, we find a surprising result: the incremental binding energy increases further to a value of 0.552 eV. This increase is the result of a water network forming around the CO_2 inside the narrow ultramicropore of TIFSIX-3-Ni (Figure S20). Such networks have been observed in other MOFs[28,41,42] but we are unaware that they have been recognized in ultramicropores. Such network formation is also observed without CO_2 (Figures S22 and S23). Adsorption of up to three water molecules is energetically favorable and we see a similar drop for the second incremental binding energy, followed by a noticeable increase for the third water added (Table 1). The binding energy per hydrogen bond of gas-phase water dimers and trimers is on the order of 0.22 eV,[43] indicating that the second and third water added to the pore (with incremental binding energies around 2–3 times that value) also have significant interactions with the MOF. Importantly, the incremental binding energy for any loading of water (with or without CO_2) is sufficient to retain water at room temperature.

Conclusion

Although the presence of moisture is typically antagonistic to the regenerable uptake and release of gases by MOM adsorbents, we reveal herein that, by using a shortened adsorption cycle on TIFSIX-3-Ni, CO_2 can be captured and released in water-saturated conditions while retaining as much as 90 % of the dry uptake, and that the performance is retained over successive cycles. Restricting water loading by curtailing the time available for adsorption leads to conditions in which ab initio calculations predict co-adsorption of CO_2 and H_2O molecules into narrow ultramicropores with higher energies than the corresponding water-only states. This is borne out by in situ FTIR studies showing that CO_2 and H_2O can indeed simultaneously occupy different binding sites within a single TIFSIX-3-Ni ultramicropore. At higher water loadings our calculations predict the formation of energetically favourable water networks, resulting in displacement of CO_2, in agreement with equilibrium DCB results. Our findings challenge the hypothesis that materials with narrow pores are unsuitable for adsorbing multiple sorbates due to steric hindrance and/or molecular competition, and outlines a strategy to minimize the detrimental impact of moisture on CO_2 uptake.[44] The detailed mechanistic information derived from our combined experimental/computational study can foster the design and synthesis of physisorbents with the right pore size and chemistry to target CO_2 capture from both dry and wet feedstocks.

Acknowledgements

Work in the US was entirely supported by the U.S. Department of Energy under award DE-SC0019902. M.J.Z. acknowledges the Science Foundation Ireland (awards 13/RP/B2549 and 16/IA/4624) and European Research Council under the European Union's H2020 research and innovation program (grant agreement ADG 885695) for sample synthesis. S.M. acknowledges an SFI-IRC Pathways award (21/PATH-S/9454) from Science Foundation Ireland.

Conflict of Interest

The authors declare no conflict of interest.

Data Availability Statement

The data that support the findings of this study are available from the corresponding author upon reasonable request.

Keywords: Carbon Capture · Co-Adsorption · Metal–Organic Frameworks · Pyrazine · Ultramicroporous Materials

[1] International Energy Agency, *Energy Technology Perspectives 2010: Scenarios & Strategies to 2050*, **2010**.
[2] E. D. Bates, R. D. Mayton, I. Ntai, J. H. Davis, *J. Am. Chem. Soc.* **2002**, *124*, 926–927.
[3] T. M. McDonald, J. A. Mason, X. Kong, E. D. Bloch, D. Gygi, A. Dani, V. Crocellà, F. Giordanino, S. O. Odoh, W. S. Drisdell, B. Vlaisavljevich, A. L. Dzubak, R. Poloni, S. K. Schnell, N. Planas, K. Lee, T. Pascal, L. F. Wan, D. Prendergast, J. B. Neaton, B. Smit, J. B. Kortright, L. Gagliardi, S. Bordiga, J. A. Reimer, J. R. Long, *Nature* **2015**, *519*, 303–308.
[4] K. Sumida, D. L. Rogow, J. A. Mason, T. M. McDonald, E. D. Bloch, Z. R. Herm, T. H. Bae, J. R. Long, *Chem. Rev.* **2012**, *112*, 724–781.
[5] M. Oschatz, M. Antonietti, *Energy Environ. Sci.* **2018**, *11*, 57–70.
[6] C. A. Trickett, A. Helal, B. A. Al-Maythalony, Z. H. Yamani, K. E. Cordova, O. M. Yaghi, *Nat. Rev. Mater.* **2017**, *2*, 17045.
[7] J. Liu, P. K. Thallapally, B. P. Mc Grail, D. R. Brown, J. Liu, *Chem. Soc. Rev.* **2012**, *41*, 2308–2322.
[8] S. R. Caskey, A. G. Wong-Foy, A. J. Matzger, *J. Am. Chem. Soc.* **2008**, *130*, 10870–10871.

[9] S. Zuluaga, E. M. A. Fuentes-Fernandez, K. Tan, F. Xu, J. Li, Y. J. Chabal, T. Thonhauser, *J. Mater. Chem. A* **2016**, *4*, 5176–5183.
[10] J. M. Kolle, M. Fayaz, A. Sayari, *Chem. Rev.* **2021**, *121*, 7280–7345.
[11] Z. Hu, Y. Wang, B. B. Shah, D. Zhao, *Adv. Sustainable Syst.* **2019**, *3*, 1800080.
[12] R. Aniruddha, I. Sreedhar, B. M. Reddy, *J. CO2 Util.* **2020**, *42*, 101297.
[13] E. J. Kim, R. L. Siegelman, H. Z. H. Jiang, A. C. Forse, J.-H. Lee, J. D. Martell, P. J. Milner, J. M. Falkowski, J. B. Neaton, J. A. Reimer, S. C. Weston, J. R. Long, *Science* **2020**, *369*, 392–396.
[14] S. Xiang, Y. He, Z. Zhang, H. Wu, W. Zhou, R. Krishna, B. Chen, *Nat. Commun.* **2012**, *3*, 954.
[15] P.-Q. Liao, H. Chen, D.-D. Zhou, S.-Y. Liu, C.-T. He, Z. Rui, H. Ji, J.-P. Zhang, X.-M. Chen, *Energy Environ. Sci.* **2015**, *8*, 1011–1016.
[16] A. M. Fracaroli, H. Furukawa, M. Suzuki, M. Dodd, S. Okajima, F. Gándara, J. A. Reimer, O. M. Yaghi, *J. Am. Chem. Soc.* **2014**, *136*, 8863–8866.
[17] P. Nugent, E. G. Giannopoulou, S. D. Burd, O. Elemento, E. G. Giannopoulou, K. Forrest, T. Pham, S. Ma, B. Space, L. Wojtas, M. Eddaoudi, M. J. Zaworotko, *Nature* **2013**, *495*, 80–84.
[18] A. Kumar, D. G. Madden, M. Lusi, K. Chen, E. A. Daniels, T. Curtin, J. J. Perry, M. J. Zaworotko, *Angew. Chem. Int. Ed.* **2015**, *54*, 14372–14377; *Angew. Chem.* **2015**, *127*, 14580–14585.
[19] S. Mukherjee, M. J. Zaworotko, *Trends Chem.* **2020**, *2*, 506–518.
[20] O. Shekhah, Y. Belmabkhout, Z. Chen, V. Guillerm, A. Cairns, K. Adil, M. Eddaoudi, *Nat. Commun.* **2014**, *5*, 4228.
[21] S. K. Elsaidi, M. H. Mohamed, H. T. Schaef, A. Kumar, M. Lusi, T. Pham, K. A. Forrest, B. Space, W. Xu, G. J. Halder, J. Liu, M. J. Zaworotko, P. K. Thallapally, *Chem. Commun.* **2015**, *51*, 15530–15533.
[22] P. M. Bhatt, Y. Belmabkhout, A. Cadiau, K. Adil, O. Shekhah, A. Shkurenko, L. J. Barbour, M. Eddaoudi, *J. Am. Chem. Soc.* **2016**, *138*, 9301–9307.
[23] O. Shekhah, Y. Belmabkhout, K. Adil, P. M. Bhatt, A. J. Cairns, M. Eddaoudi, *Chem. Commun.* **2015**, *51*, 13595–13598.
[24] S. Mukherjee, N. Sikdar, D. O'Nolan, D. M. Franz, V. Gascón, A. Kumar, N. Kumar, H. S. Scott, D. G. Madden, P. E. Kruger, B. Space, M. J. Zaworotko, *Sci. Adv.* **2019**, *5*, eaax9171.
[25] A. Kumar, C. Hua, D. G. Madden, D. O'Nolan, K.-J. Chen, L.-A. J. Keane, J. J. Perry, M. J. Zaworotko, *Chem. Commun.* **2017**, *53*, 5946–5949.
[26] D. O'Nolan, A. Kumar, M. J. Zaworotko, *J. Am. Chem. Soc.* **2017**, *139*, 8508–8513.
[27] K. Tan, S. Zuluaga, Q. Gong, Y. Gao, N. Nijem, J. Li, T. Thonhauser, Y. J. Chabal, *Chem. Mater.* **2015**, *27*, 2203–2217.
[28] K. Tan, S. Zuluaga, Q. Gong, P. Canepa, H. Wang, J. Li, Y. J. Chabal, T. Thonhauser, *Chem. Mater.* **2014**, *26*, 6886–6895.
[29] K. Lee, J. D. Howe, L.-C. Lin, B. Smit, J. B. Neaton, *Chem. Mater.* **2015**, *27*, 668–678.
[30] A. Policicchio, M. Florent, A. Celzard, V. Fierro, J. Jagiello, T. J. Bandosz, *Microporous Mesoporous Mater.* **2020**, *309*, 110571.
[31] J.-B. Lin, T. T. T. Nguyen, R. Vaidhyanathan, J. Burner, J. M. Taylor, H. Durekova, F. Akhtar, R. K. Mah, O. Ghaffari-Nik, S. Marx, N. Fylstra, S. S. Iremonger, K. W. Dawson, P. Sarkar, P. Hovington, A. Rajendran, T. K. Woo, G. K. H. Shimizu, *Science* **2021**, *374*, 1464–1469.
[32] Y. Wang, M. D. LeVan, *J. Chem. Eng. Data* **2010**, *55*, 3189–3195.
[33] N. S. Wilkins, J. A. Sawada, A. Rajendran, *Adsorption* **2020**, *26*, 765–779.
[34] K. Tan, S. Zuluaga, E. Fuentes, E. C. Mattson, J. F. Veyan, H. Wang, J. Li, T. Thonhauser, Y. J. Chabal, *Nat. Commun.* **2016**, *7*, 13871.
[35] S. Mukherjee, N. Kumar, A. A. Bezrukov, K. Tan, T. Pham, K. A. Forrest, K. A. Oyekan, O. T. Qazvini, D. G. Madden, B. Space, M. J. Zaworotko, *Angew. Chem. Int. Ed.* **2021**, *60*, 10902–10909; *Angew. Chem.* **2021**, *133*, 10997–11004.
[36] D. J. Tranchemontagne, J. R. Hunt, O. M. Yaghi, *Tetrahedron* **2008**, *64*, 8553–8557.
[37] J. H. Cavka, S. Jakobsen, U. Olsbye, N. Guillou, C. Lamberti, S. Bordiga, K. P. Lillerud, *J. Am. Chem. Soc.* **2008**, *130*, 13850–13851.
[38] K. Li, D. H. Olson, J. Seidel, T. J. Emge, H. Gong, H. Zeng, J. Li, *J. Am. Chem. Soc.* **2009**, *131*, 10368–10369.
[39] Y. Chen, Z. Qiao, J. Huang, H. Wu, J. Xiao, Q. Xia, H. Xi, J. Hu, J. Zhou, Z. Li, *ACS Appl. Mater. Interfaces* **2018**, *10*, 38638–38647.
[40] A. Ö. Yazaydın, A. I. Benin, S. A. Faheem, P. Jakubczak, J. J. Low, R. R. Willis, R. Q. Snurr, *Chem. Mater.* **2009**, *21*, 1425–1430.
[41] S. Zuluaga, E. M. A. Fuentes-Fernandez, K. Tan, J. Li, Y. J. Chabal, T. Thonhauser, *J. Mater. Chem. A* **2016**, *4*, 11524–11530.
[42] N. Nijem, P. Canepa, U. Kaipa, K. Tan, K. Roodenko, S. Tekarli, J. Halbert, I. W. H. Oswald, R. K. Arvapally, C. Yang, T. Thonhauser, M. A. Omary, Y. J. Chabal, *J. Am. Chem. Soc.* **2013**, *135*, 12615–12626.
[43] B. Kolb, T. Thonhauser, *Phys. Rev. B* **2011**, *84*, 045116.
[44] R.-B. Lin, L. Li, H.-L. Zhou, H. Wu, C. He, S. Li, R. Krishna, J. Li, W. Zhou, B. Chen, *Nat. Mater.* **2018**, *17*, 1128–1133.

Manuscript received: May 5, 2022
Accepted manuscript online: June 23, 2022
Version of record online: July 8, 2022